

# SEISMIC PERFORMANCE OF CONCRETE FRAMES REINFORCED WITH SUPERELASTIC SHAPE MEMORY ALLOYS

**M.A. YOUSSEF\*, M.A. ELFEKI**

The University of Western Ontario, Department of Civil and Environmental Engineering, London, ON N6A 5B9, Canada

\*Phone: 519-661-2111 Ext. 88661, E-mail: [youssef@uwo.ca](mailto:youssef@uwo.ca)

Reinforced concrete (RC) framed buildings dissipate the seismic energy through yielding of the reinforcing bars. This yielding jeopardizes the serviceability of these buildings as it results in residual lateral deformations. Superelastic Shape Memory Alloys (SMAs) can recover inelastic strains by stress removal. Since SMA is a costly material, this paper defines the required locations of SMA bars in a typical RC frame to optimize its seismic performance in terms of damage scheme and seismic residual deformations. The intensities of five earthquakes causing failure to a typical RC six-storey building are defined and used to evaluate seven SMA design alternatives.

Keywords: Seismic Damage, Seismic Residual Deformations, Shape Memory Alloy, Superelasticity, Moment Frame, Reinforced Concrete.

## **Introduction**

Recent research has focused on reducing residual lateral deformations using re-centring devices [Valente et al., 1999], passive energy dissipating devices [Clark et al., 1995], and Shape Memory Alloys (SMAs) [Alam et al., 2009]. Sakai et al. [2003] have studied the self-restoration of concrete beams reinforced with superelastic SMA wires. Their experimental results show that mortar beams reinforced with SMA wires recover their inelastic deformations almost completely

after releasing the load corresponding to the crushing state. Saiidi and Wang [2006] have used shake table tests to evaluate the seismic performance of RC columns reinforced with SMA bars in the plastic hinge area. Their results show that SMA RC columns are able to recover nearly all of their post-yield deformations, thus requiring minimal repair. They can also withstand earthquakes with higher amplitudes as compared to conventional columns. Wang [2004] has used shake table tests to investigate the seismic performance of a damaged SMA RC column after repairing using Engineering Cementitious Composites (ECC). The study showed that the use of ECC/SMA combination has reduced the concrete damage substantially, thus requiring minimal repair even after a very large earthquake. Youssef et al. [2008] and Alam et al. [2008] have utilized superelastic SMA in the plastic hinge area of beam-column joints and have conducted experimental/analytical investigations to evaluate SMAs' performance under reversed cyclic loading. Their results show that SMA RC joints are superior to steel RC joints because of their re-centring capability. The implications of using SMA bars on the design of RC elements was examined by Elbahy et al. [2009, 2010a, 2010b]. Revised stress block parameters to estimate their flexural capacities and revised equations to assess their deformations were introduced.

Alam et al. [2009] have used dynamic analysis to assess the seismic performance of an eight-storey SMA RC frame. SMA bars have been utilized in the plastic hinge areas of all beams. The SMA RC frame has the advantage of reduced Residual Inter-storey Drifts (RIDs). However, it experiences higher Maximum Inter-storey Drifts (MIDs) due to the low modulus of elasticity of SMA. This study examines the possibility of maintaining the benefit of reduced RIDs using fewer SMA bars, thus reducing the associated costs and the increase in MIDs. Incremental dynamic analyses are performed for a typical steel RC framed building using five earthquake records. The building is then redesigned using SMA bars in the identified critical locations.

Seven different arrangements for the SMA bars are selected resulting in seven different frames. Nonlinear dynamic analyses are then conducted to select the frame which has the best seismic performance in terms of the amount and severity of damage, the Maximum Inter-storey Drift (MID), and the Maximum RID (MRID). A comprehensive study is then conducted using Incremental Dynamic Analyses (IDA) to compare the seismic performance of the steel RC frame and the selected SMA RC frame in terms of lateral capacity, MID, MRID, and earthquake intensity at collapse.

## **Superelastic SMA**

Superelasticity is a distinct property that makes SMA a smart material. A superelastic SMA can undergo large deformations and regain its initial shape after removal of stress [Saadat et al., 1999; [DesRoches et al., 2004](#)]. Ni-Ti has appeared to be the most appropriate SMA among various composites for structural applications because of its large recoverable strain, superelasticity, energy dissipation, excellent low/high fatigue properties, and exceptionally good corrosion resistance. The phase change of this alloy can be stress-induced at room temperature if the alloy has the appropriate formulation and treatment [[DesRoches and Delemont, 2002](#)]. In this study, unless otherwise stated, SMA refers to Ni-Ti SMA (commonly known as Nitinol).

Figure 1 shows a simplified model for the stress–strain relationship of SMA [Alam et al., 2007; McCormick et al., 1993; [Elbahy et al., 2009](#)]. For structural applications, it is recommended to design SMA RC sections to behave within the superelastic range [[Youssef et al., 2008](#)]. Thus, the yield stress recommended for the design should be equal to  $f_{cr}$  [Elbahy et al.,

2009]. Within the superelastic strain range, SMA dissipates specific amount of seismic energy without permanent deformations. This dissipation results from the phase transformation from austenite to martensite during loading and reverse transformation during unloading. In earthquake engineering, the energy dissipation provided by a system is usually measured using equivalent viscous damping. The equivalent viscous damping refers to the energy dissipated per cycle divided by the product of 4 and the strain energy for a complete cycle. SMA damping capacity is affected by the bar diameter and loading rate [McCormick et al., 2006]. Large diameter SMA bars have significantly lower damping capacity than SMA wires. The SMA damping capacity decreases with an increase in the loading rate [McCormick et al., 2006].

Several researchers have proposed uniaxial phenomenological models for SMA. These models have been implemented in a number of Finite Element (FE) packages, e.g. ANSYS [2005] and Seismostruct [Seismosoft, 2008]. The superelastic part of the 1D model shown in Figure 1 is used in these FE packages [Auricchio et al., 1997] where the model have been defined using six different parameters:  $f_{cr}$ ,  $f_{P1}$ ,  $f_{T1}$ ,  $f_{T2}$ ,  $E_{cr}$  and superelastic plateau strain ( $\epsilon_s$ ). Although this simplified model has been implemented in many FE programs, its suitability for seismic applications remains questionable as it does not account for the effect of the strain rate [Bassem and Desroches, 2008]. The following section gives details about the finite element program and provides an assessment of the accuracy of SMA model that is used in this study.

## Finite Element Program

The finite element program Seismostruct [Seismosoft, 2008] is selected to be used in this study. The program takes into account both geometric and material nonlinearities. It models the spread of material inelasticity along the member length and across the section area through the employment of a fibre modelling approach. The sectional stress-strain state of beam-column elements is obtained through the integration of the nonlinear uniaxial stress-strain response of the individual fibres in which the section has been subdivided. The spread of inelasticity along member length then comes as a product of the inelastic cubic formulation suggested by [Izzuddin \[1991\]](#). Two integration Gauss points per element are used for the numerical integration of the governing equations of the cubic formulation. Concrete and steel are represented using Martinez-Rueda and Elnashai model [1997], and a bilinear kinematic strain hardening model, respectively. The SMA is represented using the model of Auricchio et al. [1997].

The ability of Seismostruct to predict the dynamic behaviour of RC buildings was evaluated by Alam et al. [2009]. The three storey building tested by Bracci et al. [1992] was modeled and subjected to ground accelerations of 0.2g and 0.3g of the 1952 Taft Earthquake (N21E component). The validation was performed in terms of structural periods and global top storey displacement-time histories. The maximum difference between the numerically evaluated periods and the experimental ones was 6%. At 0.2g, the numerically evaluated maximum top-storey drift varied from the experimental results by 1.5% and 5.5% in the forward and reverse directions, respectively. At 0.3g, the forward and reverse maximum top-storey drift values varied from the experimental results by 1.7% and 1.2%, respectively [Alam et al., 2009].

The accuracy of Seismostruct in estimating the peak and residual drifts at failure is investigated by using the experimental measurements for the single cantilever column tested by Sakai and Mahin [2004]. The column is subjected to two of the components of the Los Gatos Earthquake (Loma Prieta 1989) scaled by factors of 0.7 and 1.0 [Sakai and Mahin, 2005]. Table 1 shows a comparison between the experimental and analytical results. The maximum and residual drifts are predicted with suitable accuracy, maximum error of 15.38%.

The FE program uses the simplified SMA material model of Auricchio and Sacco [1997] which does not account for the strain rate effect. Thus, its ability to predict the performance of SMA RC elements under dynamic loads requires investigation. This simplified SMA material model is used to calculate the hysteretic damping of a 12.7 mm SMA bar assuming different SMA strain values. McCormick et al. [2006] have conducted cyclic tension tests on a similar bar using a loading rate of 1.0 hz to simulate a typical seismic load effect. The values of the equivalent viscous damping obtained experimentally and analytically are compared in Figure 2. It can be noted that the performance of the simplified model is acceptable. For SMA wires, the effect of loading rate is more pronounced and further investigation is needed to judge on the capability of the model.

Alam et al. [2008] used Seismostruct to simulate the SMA beam-column joint tested by Youssef et al. [2008] under reversed cyclic loading and the SMA RC column tested by Saiidi et al. [2006] under dynamic loading. The SMA bars were connected to the steel bars with mechanical couplers for both specimens. The numerical results showed that the FE program can simulate the behaviour of SMA RC elements with reasonable accuracy. The maximum error in

the analytical predictions was 11% in the case of the SMA beam-column joint and 6.1% in the case of the SMA RC column [Alam et al., 2008].

## **Steel RC Frame Characteristics and Modeling**

A symmetric six-storey RC office building (Frame 1) is selected for this study. The selected dimensions and layout of the building are shown in Figure 3. The building is designed according to the regulations of the International Building Code [IBC, 2006] and the ACI requirements [ACI 318, 2005] assuming that it is located in California, a high seismic region. The concrete unconfined compressive strength and the reinforcing steel yielding strength are assumed to be 28 MPa and 400 MPa, respectively. The dead loads include the weight of the structural elements and the masonry walls. The live load is assumed to be equal 4.8 kN/m<sup>2</sup>, which is a typical value for office buildings. The lateral load resisting system is composed of five special moment frames. Section dimensions and reinforcement details for a typical moment frame are given in Figure 3.

As the structure is symmetric, a two-dimensional model is used. Beams and columns are modeled using cubic elasto-plastic elements. To match the distribution of longitudinal and transverse reinforcements and to monitor the progress of local damage, beams and columns are divided into six and three elements, respectively. Cross section of each element is divided into 300 fibres. Such a modeling is similar to the model used for the explained validation cases, and thus is deemed acceptable.

The frame beams are modeled as T-sections assuming an effective flange width equal to the beam width plus 14% of the clear span [Jeong and Elnashai, 2005]. The beam-column connections are modeled using rigid elements as shown in Figure 4 for interior and edge joints.

## Failure Criteria

Local yielding of elements is defined when the tensile strain in the longitudinal reinforcement reaches the yield strain (0.002 for steel and 0.007 for SMA). A number of criteria were suggested by different researchers to define local failure of concrete members. These criteria include defining a value for ultimate curvature or crushing strain [Mwafy and Elnashai 2001]. The crushing strain is expected to depend on the type of concrete, the level of confinement, and the level of axial force. The crushing strain varies from 0.0025 to 0.006 for unconfined concrete [MacGregor and Wight, 2005] and from 0.015 to 0.05 for confined concrete [Paulay and Priestley 1992]. In this paper, crushing is assumed to occur when the confined concrete strain causes the stirrups to reach their fracture strength as proposed by Pauley and Priestley [1992], Equation 1.

$$\epsilon_{cu}(\text{confined concrete}) = \epsilon_{cu}(\text{unconfined concrete}) + \frac{1.4 \rho_s f_y V_{sm}}{K_h f_c'} \quad (1)$$

where  $\rho_s$  is the ratio of the volume of transverse reinforcement to the volume of concrete core measured to outside of the transverse reinforcement,  $f_y$  is the steel yielding stress,  $\epsilon_{sm}$  is the steel strain at maximum tensile stress, and  $K_h$  is the confinement factor.

The collapse limit has been defined by the majority of researchers using a single value of MID or RID. This has led to a wide range of proposed values for MID at collapse including 2% [Sozen,



1981], 2.5% [SEAOC, 1995], 3% [[Broderick and Elnashai, 1994](#); Kappos 1997], 4% [FEMA 273, 1997], 5.6% [[Ghobarah et al., 1998](#)], and 6% [Roufaiel and Meyer, 1983]. Dymiotis [2000] established statistical distribution of the critical storey drift at collapse using existing shake table test results of small-scale bare frames. Figure 5 shows this distribution and it is evident that the MID varies from about 3% to about 15%. Unlike MID, only a few researchers defined damage levels using RIDs. Toussi and Yao [1982] and Stephens and Yao [1987] showed that buildings are considered to be critically damaged at 1% RID. FEMA 273 [1997] introduced a value of 3% RID to define the collapse limit. In this study, building collapse is not defined using a single value of drift. The collapse state is assumed to occur when four columns located in the same storey reach the crushing state. The corresponding values of MID and RID are presented to study their variation from one record to another and their ability to define local and global damage.

## **Dynamic Analysis of the Steel RC Frame**

Eigen value analysis is performed to determine the natural periods of the frame. The periods of vibration for the first four modes are equal to 0.501, 0.177, 0.104, and 0.075 seconds, respectively. Five earthquakes records are selected to conduct the dynamic analysis. These records cover a wide range of ground motion frequencies as represented by the ratio between the peak ground acceleration and the peak ground velocity ( $A/v$  ratio). The characteristics of the chosen records are presented in Table 2. Figure 6 shows spectral acceleration for the chosen earthquakes scaled to match the design spectra at the first period of vibration. Using a reliable method to scale the selected records is critical when conducting dynamic analysis. Available methods include scaling based on: Peak Ground Acceleration (PGA), peak ground velocity, and

the 5% damped spectral acceleration at the structure's first-mode period [ $Sa(T1, 5\%)$ ]. Using  $Sa(T1,5\%)$  to scale the records was found to be a reliable method [Shome and Cornell, 1999; [Vamvatsikos and Cornell, 2002](#)].

The damage schemes at collapse under the effect of the selected records are shown in Figure 7. Table 3 presents values for  $Sa$ , MID, and MRID at collapse and defines the critical stories. It can be observed from Figure 7 that: (1) collapse occurs due to crushing of the lower ends of the first storey columns; (2) most of the beams and columns experience some degree of yielding; (3) the 4<sup>th</sup> floor beams experience the highest damage as they sustained yielding at their mid-spans under the effect of Whittier, Loma Prieta and San Fernando earthquakes, and (4) the 5<sup>th</sup> floor beams sustain yielding at their mid-spans under the effect of Whittier and Loma Prieta earthquakes. Damage to the 4<sup>th</sup> and 5<sup>th</sup> floor beams results during exposure to earthquakes that excite higher modes of vibration. Table 3 shows that the MIDs and MRIDs at collapse vary from 4.36% to 6.25% and from 2.47% to 3.00%, respectively. It can also be noted that the storey experiencing the MID is not necessarily the one experiencing the MRID. It is clear that local damage cannot be estimated using a single value of MID or MRID. The collapse drift limit suggested by FEMA (4% MID) is conservative for the studied frame and the residual drift limit (3% MRID) is un-conservative.

## **SMA RC Frames**

The analyzed steel RC frame is redesigned, in this section, using combination of steel and SMA bars. To maximize the benefit of using SMA while minimizing the instantaneous

additional cost, seven alternative locations for SMA bars are examined. These alternative locations are based on the critical sections defined by the dynamic analysis of the steel RC frame. The positions selected for the SMA bars, shown in Figure 8, are: [1] SMA bars at the ends of all beams to address the observed yielding (Frame 2), [2] SMA bars at the bottom ends of the first storey columns as they are considered the most critical columns (Frame 3), [3] SMA bars at the ends of the fourth floor beams as they are considered the most critical beams (Frame 4), [4] SMA bars at the ends of the fifth floor beams to address the excessive yielding observed at these locations (Frame 5), [5] SMA bars at the ends of the first floor beams to study the effect of using SMA bars in the beams adjacent to the critical columns (Frame 6), [6] SMA bars at the ends of the fourth and first floor beams (Frame 7), and [7] SMA bars at the ends of the first floor beams and at the bottom ends of its columns (Frame 8).

The SMA yielding stress is assumed to be 401 MPa [Alam et al., 2009]. For each frame, the SMA RC sections are redesigned using the method proposed by Elbahy et al. [2009]. This method includes:

- (1) calculating the concrete maximum strain using a chart given by Elbahy et al. [2009]. It is taken equal to 0.0035 for beam sections as they sustain very low axial loads. The axial load supported by the first floor columns is about 60% of the axial load capacity. The concrete maximum strain corresponding to this axial load level is 0.00255.
- (2) The maximum strain values are used to calculate the stress block parameters as proposed by Elbahy et al. [2009]. These parameters are used to calculate the moment capacity of the SMA RC sections.

The length of the plastic hinge ( $L_p$ ) is calculated using Equation 2 that was proposed by Paulay and Priestley [1992] and recommended for SMA RC elements by Alam et al. [2008] and Wang [2004].

$$L_p = 0.08 \cdot L + 0.022 \cdot d_{sma} \cdot f_{cr} \quad (2)$$

where  $L$  is the element length from the face of the beam-column joint to mid-span of the beam,  $d_{sma}$  is the SMA bar diameter, and  $f_{cr}$  is the yielding stress of the SMA bars. The plastic hinge length for 19 mm and 29 mm SMA bars is calculated as 390 mm and 373 mm, respectively. Mechanical couplers are assumed to connect SMA with regular steel bars as recommended by Youssef et al. [2008] and Saaidi and Wang [2006]. For the exterior joints, the lengths of the 19 mm and 29 mm SMA bars (centre to centre of the couplers) are 480 mm and 465 mm, respectively. For the interior joints, the length of the SMA bars (centre to centre of the couplers) is 1350 mm. The arrangement of couplers in a typical SMA RC beam is shown in Figure 9. Each SMA RC frame is subjected to the selected five earthquake records scaled to the intensity causing collapse of the steel RC frame. The original periods of vibrations of the SMA RC frames are similar to the steel RC frame. Under loading, concrete cracks and changes to the periods are affected by the lower modulus of SMA bars.

The values of the MID and the MRID for the studied frames are illustrated in Table 4. Figure 10 shows a comparison between their average values. The steel RC frame has the lowest MID (5.20%) and Frame 2 (SMA used at 48 sections) has the highest MID (6.42%). All the other frames have relatively similar average values of MID (varying from 5.57% to 5.77%). The percentage difference between the average values of MID and MRID for the SMA RC frames

and those for the Steel RC frame are presented in Table 4. The values show that the maximum increase in the MID demand is observed in Frame 2 (23.51%) where the SMA bars are used at 48 sections (at the end of all the beams). For other frames, this increase ranges from 7.08% for Frame 6 to 10.97% for Frame 4. Both of Frames 4 and 6 have SMA bars at eight sections. It is clear that the location of these bars has a minor effect on the value of the MID. The increase in the values of the MID for the SMA RC frames is due to low modulus of elasticity of the SMA bars, which is about one third of the steel modulus of elasticity. The average values of MRID demands show a different scenario than that observed for MID. The location of the SMA bars greatly affects the MRID demands. It can result in a significant reduction (Frames 2, 6, 7, and 8), a low reduction (Frames 3 and 5), or an increase (Frame 4) in the MRID as compared to the steel RC frame. The reductions in the average values of MRID are 76.24%, 74.54%, 65.38%, and 56.87% for Frames 2, 7, 6, and 8, respectively. A lower reduction is observed for Frame 3 (37.79%) and for Frame 5 (1.56%). The MRID has increased in Frame 4 (4.08%).

The damage schemes of the seven frames illustrated in Figures 11a to 11g show that: (1) yielding is observed at the ends of almost all beams and columns, and (2) yielding at mid-spans of the beams is mostly observed in the cases of San Fernando, Whittier, and Loma Prieta earthquakes due to an increase in the vertical deformation demand.

The damage schemes for Frame 2, Figure 11a, show that: (1) crushing can be observed in the first storey columns in the case of San Fernando, and (2) in the case of Whittier, the frame can be considered at collapse state where four of the first storey column sections and five of the third storey column sections sustained crushing.

The damage schemes for Frame 3, Figure 11b, show that: (1) crushing is only observed at the first storey columns, (2) in the case of Whittier earthquake, crushing is observed at the ends

of five columns and the frame reached collapse at the same PGA as that of Frame 1, and (3) for the other four records, Frame 3 did not collapse and can sustain higher PGA than Frame 1.

The damage schemes of Frame 4, Figure 11c, show that: (1) crushing is concentrated at the first storey columns, and (2) the building can be considered at collapse state in case of three earthquakes (Imperial Valley, Northridge, and Whittier) where four of the first storey columns have experienced crushing.

The damage schemes of Frame 5, Figure 11d, shows that: (1) crushing is concentrated at the first storey columns, (2) two of the third storey columns reach crushing at their top end in the case of Whittier record, (3) the frame is at collapse state in the case of Northridge, San Fernando, and Whittier records, and (4) for the other two records, it can tolerate higher seismic intensities.

The damage schemes of Frame 6, Figure 11e, show that: (1) crushing is observed at the first storey columns in three earthquakes, (2) no crushing is observed at higher storey columns, (3) while the building is considered at the collapse state in the case of Whittier earthquake, it can sustain higher intensities for the other four earthquakes, (4) using SMA at the ends of the first floor beams only (Frame 6) produces a similar damage scheme to Frame 2 (SMA at the ends of all the beams).

The damage schemes of Frame 7, Figure 11f, show that: (1) crushing is only observed at the first storey columns, and (2) under the effect of all the earthquake records used, the frame does not reach the collapse state and can tolerate higher earthquake intensities.

The damage schemes of Frame 8, Figure 11g, show that: (1) the performance of Frame 8 (SMA bars at the first storey beams and columns) is better than Frame 3 (SMA at columns of the first storey), (2) the number of crushed columns is reduced in San Fernando, Whittier and

Imperial Valley cases, and (3) the frame is considered at the collapse state in the case of Whittier record.

It is clear from the damage schemes and the drift values, that using a reasonable amount of SMAs at the right locations leads to a lower level of damage, a minor increase in the MID, and a high reduction in the MRID as compared to a steel RC frame. Frame 7 is considered to have the best seismic performance as it has the best damage scheme, a minor increase in MID demands, and a high reduction in the MRID. The frame can also tolerate earthquakes with higher intensities. By comparing the MRID results with the damage schemes in Figure 11, it can also be observed that the frames with high values of MRID (Frames 4 and 5) have reached the collapse state under the effect of a minimum of three records. Frames 2, 6, 7 and 8, which have low values of MRID, can tolerate higher earthquake intensities for at least four of the records. MRID is clearly related to the damage state of the building. A comprehensive comparison between the seismic performance of Frames 1 and 7 is presented in the following section.

### **Steel RC Frame (Frame 1) Versus SMA RC Frame (Frame 7)**

Results of Incremental Dynamic Analysis (IDA) are presented in Figures 12a, 12c, and 12e for Frame 1 and in Figures 12b, 12d, and 12f for Frame 7. Figures 12a and 12b show that using SMA bars has a minor effect on the frame lateral capacity (the maximum base shear demand). It results in an average reduction of the frame lateral capacity of about 6.8%.

Figures 12c, 12e, 12d, and 12f show that: (1) Frames 1 and 7 have almost the same values of MIDs and MRIDs at low levels of  $S_a$ , (2) Frame 7 experiences slightly higher values of MIDs

than Frame 1 at high level of  $S_a$  (increase of 9.27% at  $S_a$  causing failure to Frame 1), and (3) Frame 7 experiences significantly lower values of MRIDs than Frame 1 at high levels of  $S_a$  (decrease of 74.54% at  $S_a$  causing failure to Frame 1).

Loma Prieta earthquake is chosen to provide additional discussion in this section. Figures 13a and 13b show that the steel and the SMA frames have almost the same values of MID and MRID ratios for  $S_a$  values less than 2.0 g. For higher values of  $S_a$ , the MID ratios of the SMA frame are higher than those of the steel frame. The maximum difference is observed at 3.0g  $S_a$  where the MID of Frames 1 and 7 are 4.4% and 5.85%, respectively. Figure 13b shows that the re-centring effect of the SMA is very significant. At high levels of  $S_a$ , the MRIDs of the steel frame have reached values higher than 2.3% while those for Frame 7 are lower than 0.5%.

A comparison of the damage scheme of the two buildings at the same level of  $S_a$  (Figures 7 and 11f), reveals that while the steel frame is at the collapse state, the SMA frame is not at the collapse state and can tolerate higher levels of  $S_a$ . Table 5 summarizes the  $S_a$  that causes collapse to Frame 7, the corresponding MID, and MRID. The damage schemes of Frame 7 at collapse are presented in Figure 14. The collapse of the SMA frame is similar to that of the steel frame where four of the first storey columns are crushed. Using SMA bars has resulted in spreading the local damage (yielding and crushing) to include higher stories. For example, column crushing is observed at the third and fourth stories in the cases of San Fernando, Loma Prieta, and Northridge records. The spreading of the damage has led to higher energy dissipation and higher seismic capacity. It can be observed from Table 5 that  $S_a$  values causing collapse of the SMA frame are much higher than those causing collapse of the steel RC frame (Table 3). Table 5 also shows that at collapse, the MID varies from 5.7% to 7.64% and the MRID varies



from 1.00% to 4.00%. By comparing these values to those obtained for the steel RC frame (Table 3), it can be concluded that the SMA frame is more ductile than the steel frame, undergoes higher maximum drifts, and has lower permanent drifts.

## **Summary and Conclusions**

This paper optimizes the use of smart material, SMA, in RC frames to achieve the best seismic performance in terms of: damage scheme, lower MRIDs, and reasonable values of MID. The accuracy of the used finite element program is validated for steel and SMA RC sections. The SMA model proposed by Auricchio and Sacco (1997) is found to be acceptable in providing good estimates for the damping capacity of large diameter SMA bars.

A six-storey RC frame building located in a highly seismic zone is considered as a case study. The building is subjected to nonlinear dynamic analyses using five different earthquake records scaled to different  $S_a$  levels. After defining the position of the critical sections in the building, seven different alternative designs that utilize SMA bars are tested. These seven alternatives are subjected to nonlinear dynamic analysis using the same records scaled to the predefined  $S_a$  level that caused collapse of the steel RC frame. The building having the least damage, low values of MRID, and reasonable MID values is selected. A comparative study is then carried out between the seismic performance of the steel RC frame and the selected SMA RC frame.

Failure of the steel RC frame has resulted from crushing of the columns in the first storey. The largest number of yielded sections has been observed in the beams of the 4<sup>th</sup> and the

5<sup>th</sup> floors. The building's deformations showed that the MID representing the collapse varied between 4.36% and 6.25% showing that the value (4.00% MID) suggested by FEMA is conservative. However, the MRID obtained from the analyses varied between 2.47% and 3.00% showing that the value suggested by the FEMA for permanent drift (3.00% MRID) is unconservative. The analyses for the steel RC frame have confirmed that using a single value of MID or MRID is not capable of estimating the position of local damage.

The dynamic analyses conducted for the seven SMA frames during this study resulted in the following conclusions: (1) using SMA bars in the critical beams or the critical columns does not lead to good enhancement of the building seismic performance, (2) using SMA bars at the ends of all the beams increases the seismic capacity of the frame and reduces the seismic residual deformations but it significantly increases the instantaneous drifts, (3) using the SMA bars at the ends of beams adjacent to the critical columns (first floor beams) has led to very good values of MRID and prevented the building from reaching the collapse state in four out of five ground motion records, (4) The best arrangement of SMA bars in the building is found to be a combination of using them at the critical sections of the beams, 4<sup>th</sup> floor beams, and using the SMA at the beam ends adjacent to the critical columns, 1<sup>st</sup> floor beams (Frame 7), and (5) The MID values are affected by the amount of SMA bars used in the building, while the damage and the MRIDs depend on the location of these bars.

The comparison between the performance of the selected SMA RC frame (Frame 7) and the performance of the steel RC frame (Frame 1) has led to the following conclusions: (1) the SMA frame experiences slightly higher values of MID than those of the steel RC frame, (2) using SMA has significantly reduced the MRID of the frame under the effect of all records, (3)

the SMA frame has a lower number of crushed columns, and (4) the SMA frame is able to sustain higher earthquake intensities.

## References

- ACI 318 [2005] “Building Code Requirements for Structural Concrete (ACI 318-05) and commentary (ACI 318R-05),” American Concrete Institute, Farmington Hills MI, USA.
- Alam, M.S., Youssef, M.A. and Nehdi, M. [2007] “Utilizing shape memory alloys to enhance the performance and safety of civil infrastructure: a review,” *Canadian Journal of Civil Engineering* 34(9): 1075–1086.
- Alam, M.S., Youssef, M.A. and Nehdi, M. [2008] "Analytical prediction of the seismic behaviour of superelastic shape memory alloy reinforced concrete elements," *Engineering Structures* 30(12): 3399-3411.
- Alam, M.S., Nehdi, M. and Youssef, M.A. [2009] "Seismic Performance of Concrete Frame Structures Reinforced with Superelastic Shape Memory Alloys," *Smart Structures and Systems* 5(5): 565-585.
- ANSYS [2005], Version 10.0, ANSYS, Inc., Canonsburg, PA, USA.
- Auricchio, F. and Sacco, E. [1997] “Superelastic shape-memory-alloy beam model,” *Journal of Intelligent Material Systems and Structures* 8(6): 489-501.
- Auricchio, F., Taylor, R.L. and Lubliner, J. [1997] “Shape-memory alloys: macromodelling and numerical simulations of the superelastic behaviour,” *Computer Methods in Applied Mechanics and Engineering* 146(3-4): 281-312.
- Bassem, A. and Desroches, R. [2008] “Sensitivity of seismic applications to different shape memory alloy models,” *Journal of Engineering Mechanics* 134(2): 173–183.

- Bracci, J. M., Reinhorn, A. M. and Mander, J. B. [1992] "Seismic resistance of reinforced concrete frame structures designed only for gravity loads: Part I - Design and properties of a one-third scale model structure," Technical Report NCEER-92-0027, State University of New York, Buffalo, USA.
- Broderick, B. M. and Elnashai, A. S. [1994] "Seismic resistance of composite beam-columns in multi-storey structures, Part 2: Analytical model and discussion of results," *Construction Steel Research* 30(3): 231–258.
- Clark, P.W., Aiken, I.D., Kelly, J.M., Higashino, M. and Krumme, R. [1995] "Experimental and analytical studies of shape-memory alloy dampers for structural control," *Proc. of Passive Damping*, San Diego, CA, USA, paper No. 2445: 241-251.
- DesRoches, R. and Delemont, M. [2002] "Seismic retrofit of simply supported bridges using shape memory alloys," *Engineering Structures* 24(3): 325-332.
- DesRoches, R., McCormick, J., and Delemont, M. [2004] "Cyclic Properties of Superelastic Shape Memory Alloy Wires and Bars," *Journal of Structural Engineering, ASCE* 130(1): 38-46.
- Dymiotis, C. [2000] "Probabilistic seismic assessment of reinforced concrete buildings with and without masonry infills," *Ph.D. thesis*, Imperial College of Science, Technology and Medicine, London, UK.
- Elbahy, Y.I., Youssef, M.A. and Nehdi, M. [2009] "Stress Block Parameters for Concrete Flexural Members Reinforced with Shape Memory Alloys," *Materials and Structures* 42(10): 1335-1351.

- Elbahy Y.I., Youssef M.A., Nehdi M., 2010a, “Deflection of Superelastic Shape Memory Alloy Reinforced Concrete Beams: Assessment of Existing Models,” *Canadian Journal of Civil Engineering* 37(6): 842-854.
- Elbahy Y.I., Nehdi M., Youssef M.A., 2010b, “Artificial Neural Network Model for Deflection Analysis of Superelastic Shape Memory Alloy RC Beams,” *Canadian Journal of Civil Engineering* 37(6): 855-865.
- FEMA 273 [1997] “NEHRP Guidelines for the Seismic Rehabilitation of Buildings,” Federal Emergency Management Agency, Washington, DC, USA.
- Ghobarah, A., Aly, N.M. and El-Attar, M. [1998] “Seismic reliability assessment of existing reinforced concrete building,” *Journal of Earthquake Engineering* 2(4): 569-592.
- IBC [2006] International Building Code, International Code Council, Country Club Hills, IL.
- Izzuddin B.A. [1991] “Nonlinear Dynamic Analysis of Framed Structures”, PhD Thesis, Imperial College, University of London, London.
- Jeong, S.H., and Elnashai, A. [2005] “Analytical assessment of an irregular RC frame for full-scale 3D pseudo-dynamic testing part I: analytical model verification,” *Earthquake Engineering* 9(1): 95-128.
- Kappos, A.J. [1997] “A comparative assessment of R/C structures designed to the 1995 Eurocode 8 and the 1985 CEB seismic code,” *The Structural Design of Tall Buildings* 6(1): 59-83.
- Martinez-Rueda, JE. and Elnashai, AS. [1997] ”Confined concrete model under cyclic load,” *Materials and Structures* 30(197): 139-147.

- McCormick, J., Desroches, R., Fugazza, D. and Auricchio, F. [2006] “Seismic vibration control using superelastic shape memory alloys,” *Journal of Engineering Material and technology* 128(3): 294-301.
- McCormick, P.G., Liu, Y. and Miyazaki, S. [1993] “Intrinsic thermalmechanical behavior associated with the stress-induced martensitic transformation of NiTi,” *Materials Science and Engineering- A- structural material* 167: 51–56.
- MacGregor, J.G. and Wight, J.K. [2005] “Reinforced Concrete Mechanics and Design,” Prentice Hall, Upper Saddle River, NJ, USA.
- Mwafy, A.M. and Elnashai, A.S. [2001] “Static pushover versus dynamic collapse analysis of RC buildings,” *Engineering Structures* 23(5): 407-424.
- Paulay, T. and Priestley, M.J.N. [1992] “Seismic design of reinforced concrete and masonry buildings,” John Wiley & Sons, New York, NY, USA.
- Roufaiel, M. S. L., and Meyer, C. [1983] “Performance based seismic design,” *Proceeding of the 12<sup>th</sup> world conference on Earthquake Engineering*, New Zealand Society for Earthquake Engineering, Auckland, New Zealand, paper ID: 2831, (on CD).
- Saadat, S., Salichs, J., Duval, L., Noori, M., Hou, Z., Baron, I., and Davoodi, H. [1999] “Utilization of Shape Memory Alloys for Structural Vibration Control,” *U.S./Japan Workshop on Smart Materials and New Technologies for Improvement of Seismic Performance of Urban Structures*, Disaster Prevention Research Institute, Kyoto University, Kyoto, Japan.
- Saiidi, MS. and Wang, H. [2006] “Exploratory study of seismic response of concrete columns with shape memory alloys reinforcement,” *ACI Structural Journal* 103(3): 435-442.

- Sakai, Y., Kitagawa, Y., Fukuta, T. and Iiba, M. [2003] “Experimental study on enhancement of self-restoration of concrete beams using SMA wire,” *Proceedings of SPIE Vol. 5057, Smart Structures and Materials, Smart Systems and Non destructive Evaluation for Civil Infrastructures*, San Diego, CA, USA , pp. 178–186.
- Sakai, J., and Mahin, S.A. [2004] “Mitigation of residual displacements of circular reinforced concrete bridge columns,” *Proceedings of the Thirteenth World Conference on Earthquake Engineering*, Vancouver, BC, Canada, Paper No. 1622. 13 pp.
- Sakai, J. and Mahin S. [2005] "Earthquake simulator tests on the mitigation of residual displacement of reinforced concrete bridge columns," *Proc., 21st US-Japan Bridge Engineering Workshop*, Tsukuba Japan, FHWA, McLean, VA, October 2005, 8 pp.
- SEAOC [1995] “Performance Based Seismic Engineering of Buildings,” Vision 2000 Committee, Structural Engineering Association of California, Sacramento, California.
- SeismoSoft [2008] "SeismoStruct - A computer program for static and dynamic nonlinear analysis of framed structures", Available from URL: <http://www.seismosoft.com>.
- Shome, N., Cornell, C.A. [1999] “Probabilistic seismic demand analysis of non-linear structures,” Report No. RMS-35, RMS Program, Stanford University, Stanford, CA.
- Sozen, M. A. [1981] “Review of Earthquake response of reinforced concrete buildings with a view to drift control,” *State-of-the-Art in Earthquake Engineering, Turkish National Committee on Earthquake Engineering*, Istanbul, Turkey, pp. 383-418.
- Stephens, J.E. and Yao, J.T.P. [1987] “Damage assessment using response measurements,” *Journal of Structural Engineering, ASCE* 113(4): 787-801.
- Toussi, S. and Yao, J. T. P. [1982] “Hysteresis identification of existing structures,” *Journal of Engineering Mechanics, ASCE* 109(5): 1189-1203.

- Valente, C., Cardone, D., Lamunaca, B.G. and Penzo, F.M. [1999] "Shaking table tests of structures with conventional and SMA based protection devices," MANSIDE Project, Italian Department for National Technical Services, Rome, Italy, 11177-11192.
- Vamvatsikos, D. and Cornell, C. A. [2002] "Incremental dynamic analysis," *Journal of Earthquake Engineering and Structural Dynamics* 31(3): 491-514.
- Wang, H. [2004] "A Study of RC Columns with Shape-Memory-Alloy and Engineered Cementitious Composites," *M.Sc. thesis*, University of Nevada, USA.
- Youssef, M.A., Alam, M.S. and Nehdi M. [2008] "Experimental investigation on the seismic behaviour of beam-column joints reinforced with superelastic shape memory alloys," *Journal of Earthquake Engineering* 12(7): 1205-1222.



Table 1: Predictions of the FE program for the experimental work by Sakai and Mahin [2005]

	70% Scale				100% Scale			
	N-S Direction		E-W direction		N-S Direction		E-W direction	
	Maximum	Residual	Maximum	Residual	Maximum	Residual	Maximum	Residual
Experimental Disp. (mm)	145.00	19.50	100.00	13.00	310.00	245.00	180.00	140.00
Analytical Disp. (mm)	125.00	16.50	95.00	11.50	280.00	246.00	180.00	140.00
Error (%)	13.79	15.38	5.00	11.50	9.68	0.41	0.00	0.00

Table 2: Chosen earthquake records

Earthquake	Date	Ms Magnitude	Station	PGA (g)	A/v
Northridge USA	17/01/94	6.7	Arleta-Nordhoff	0.340	Inter.
Imperial Valley USA	15/10/79	6.9	El Centro Array #6	0.439	Low
Loma Prieta USA	18/10/89	7.1	Capitola (CAP)	0.530	High
Whittier USA	01/10/87	5.7	Whittier Dam	0.316	High
San Fernando	09/02/71	6.6	Pacoima Dam	1.230	Inter.

Table 3: MID and MRID of the steel RC frame at failure

Earthquake record	Storey experiencing MID		Storey experiencing MRID	
	Storey No.	MID (%)	Storey No.	MRID (%)
Northridge (2.60g)	2 <sup>nd</sup>	5.13	2 <sup>nd</sup>	3.00
Imperial Valley (1.15g)	2 <sup>nd</sup>	4.36	2 <sup>nd</sup>	2.68
Loma Prieta (4.28g)	5 <sup>th</sup>	5.00	2 <sup>nd</sup>	2.72
Whittier (5.00g)	1 <sup>st</sup>	6.25	1 <sup>st</sup>	2.47
San Fernando (8.15g)	2 <sup>nd</sup>	5.25	1 <sup>st</sup>	2.60

Table 4: MID and MRID at Sa causing failure of the steel frame

	Frame 1 (Steel frame)		Frame 2 (48 SMA sections)		Frame 3 (5 SMA sections)		Frame 4 (8 SMA sections)		Frame 5 (8 SMA sections)		Frame 6 (8 SMA sections)		Frame 7 (16 SMA sections)		Frame 8 (13 SMA sections)	
	MID (%)	MRID (%)	MID (%)	MRID (%)	MID (%)	MRID (%)	MID (%)	MRID (%)	MID (%)	MRID (%)	MID (%)	MRID (%)	MID (%)	MRID (%)	MID (%)	MRID (%)
Northridge (2.60g)	5.13	3.00	5.53	0.83	5.77	1.67	7.42	3.33	5.53	3.33	5.67	0.83	5.86	1.00	5.78	1.17
Imperial Valley (1.15g)	4.36	2.68	4.37	0.20	5.08	1.6	4.32	2.52	5.09	2.33	4.42	0.67	4.06	0.73	4.38	0.67
Loma Prieta (4.28g)	5.00	2.72	6.85	0.50	4.69	1.67	5.33	2.17	5.51	2.17	4.92	1.00	5.27	0.33	4.67	0.50
Whittier (5.00g)	6.25	2.47	8.60	1.00	7.10	0.67	6.59	3.33	7.01	2.50	6.70	0.33	6.77	0.67	7.03	0.67
San Fernando (8.15g)	5.25	2.60	6.76	0.67	5.70	2.77	5.18	2.67	5.2	2.93	6.12	1.83	6.44	0.70	6.42	2.80
Average value	5.20	2.69	6.42	0.64	5.67	1.68	5.77	2.80	5.67	2.65	5.57	0.93	5.68	0.69	5.66	1.16
Percent of change *	NA	NA	23.51	-76.24	9.04	-37.79	10.97	4.08	9.04	-1.56	7.08	-65.38	9.27	-74.54	8.81	-56.87

\* The percent of change is referenced to the steel RC frame

Table 5: MID and MRID of the SMA RC frame (Frame 7) at failure

Earthquake record	Storey experiencing MID		Storey experiencing MRID	
	Storey No.	MID (%)	Storey No.	MRID (%)
Northridge (3.10g)	3 <sup>rd</sup>	7.64	3 <sup>rd</sup>	2.07
Imperial Valley (1.28g)	1 <sup>st</sup>	5.70	3 <sup>rd</sup>	1.10
Loma Prieta (5.75.g)	5 <sup>th</sup>	6.33	3 <sup>rd</sup>	1.33
Whittier (5.25g)	1 <sup>st</sup>	7.25	1 <sup>st</sup>	1.00
San Fernando (8.90g)	3 <sup>rd</sup>	7.30	3 <sup>rd</sup>	2.50

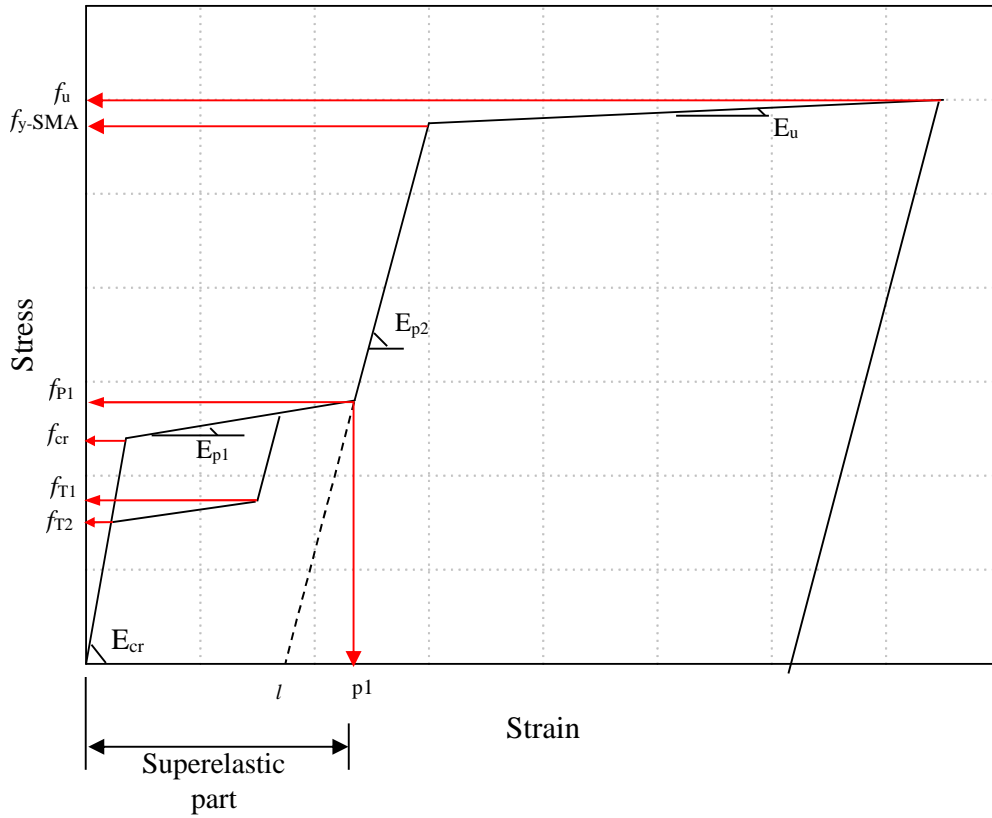


Figure 1: Typical stress-strain model for superelastic SMA

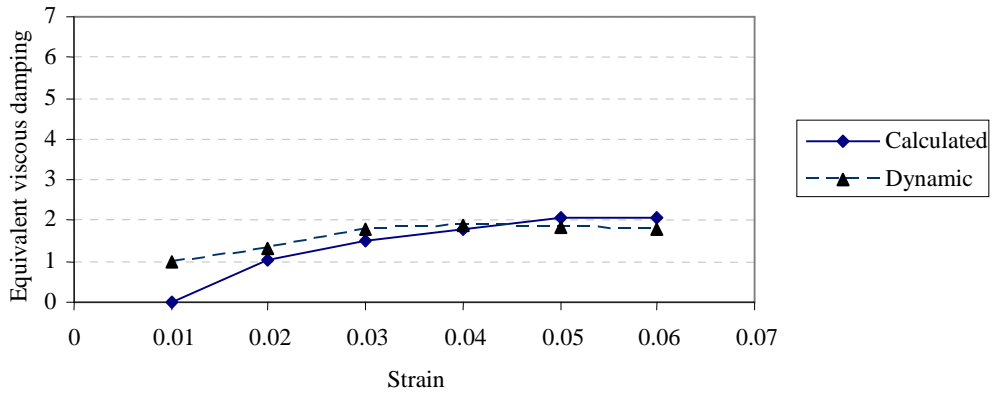
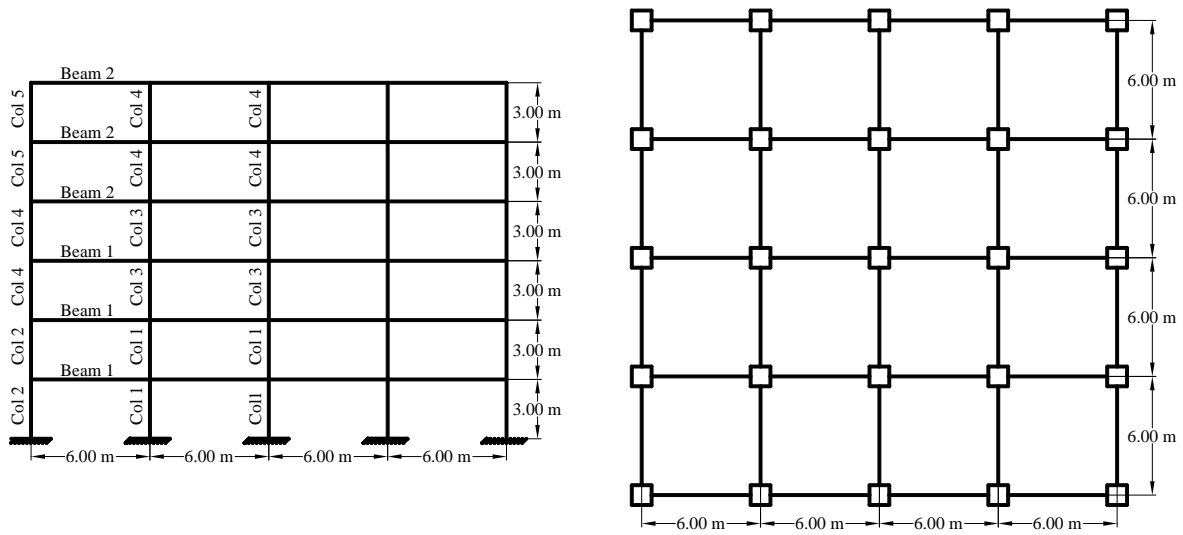
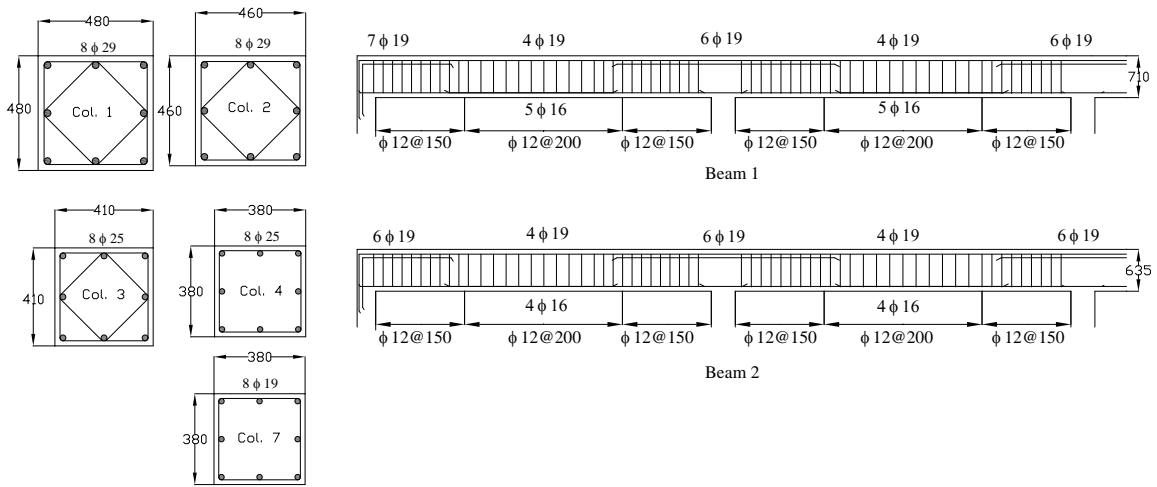


Figure 2: Equivalent viscous damping of SMA bars



Plan and Elevation



Cross sections of beams and columns

Figure 3: Six-storey RC building

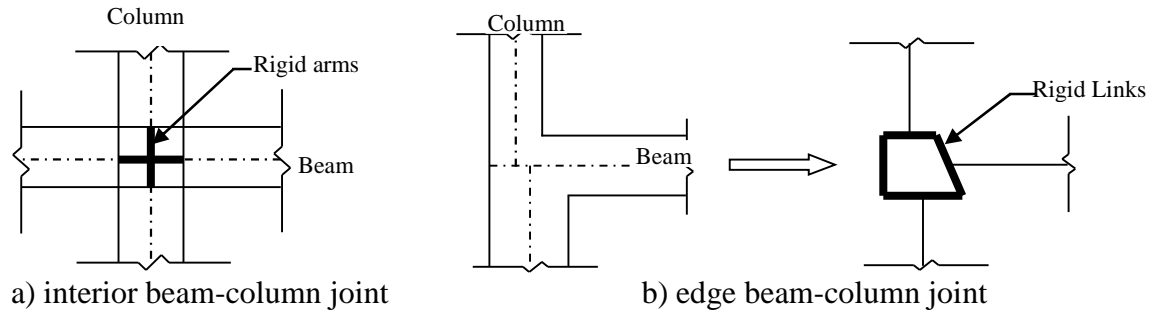


Figure 4: Modeling of beam column joints

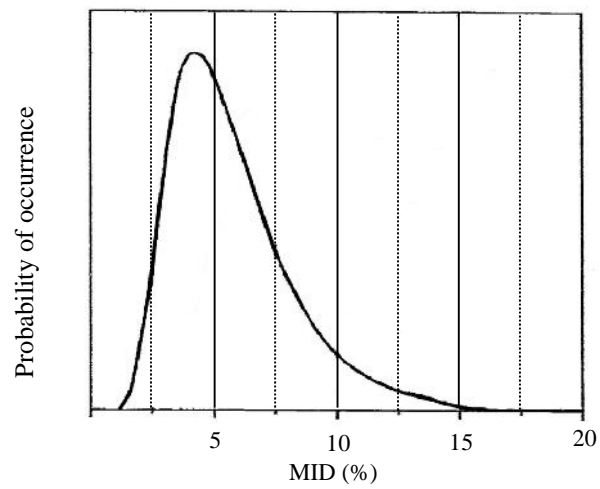


Figure 5: Distribution of ID at failure

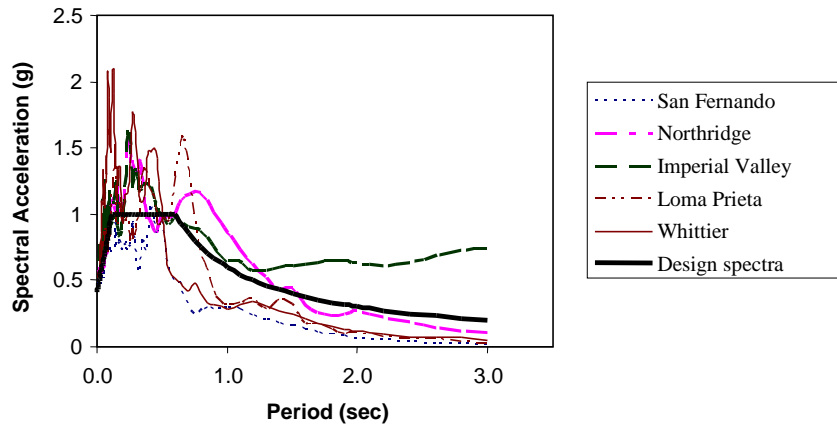
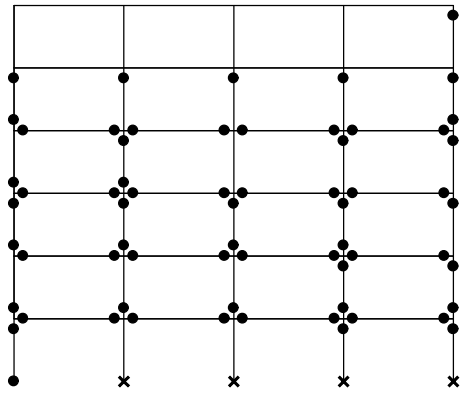
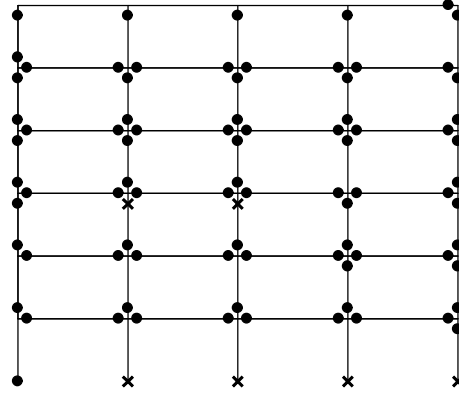


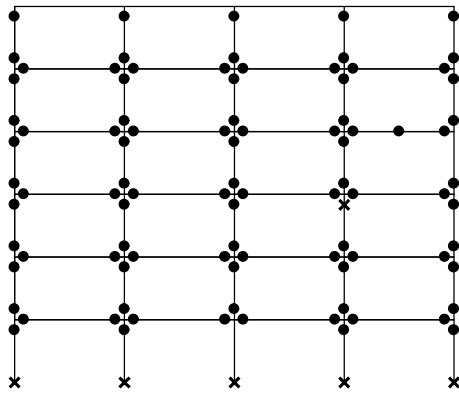
Figure 6: Spectral acceleration diagrams



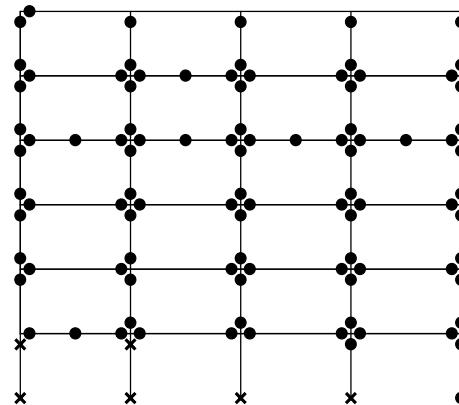
Imperial Valley (1.15 g)



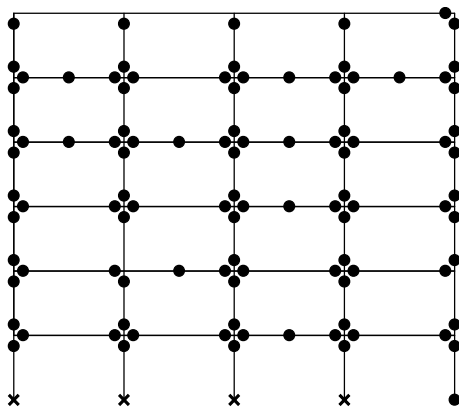
Northridge (2.60 g)



San Fernando (8.15 g)



Whittier (5.00 g)

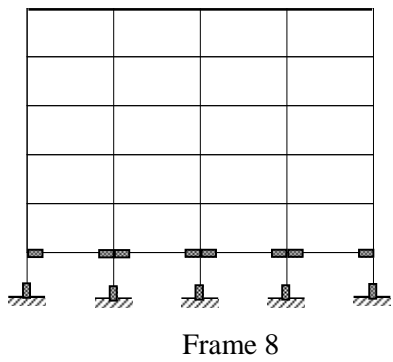
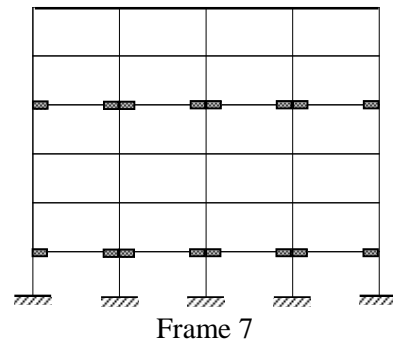
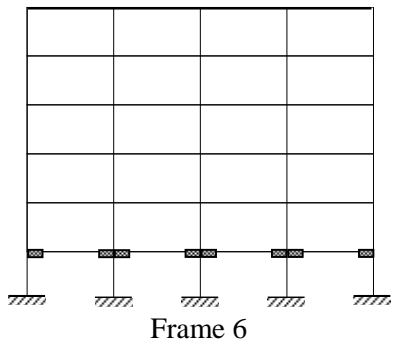
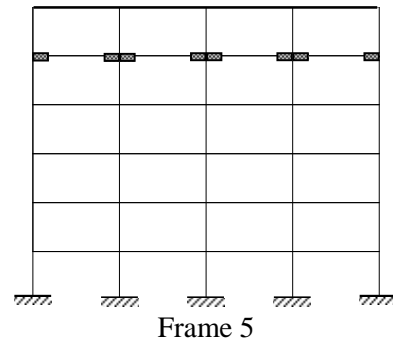
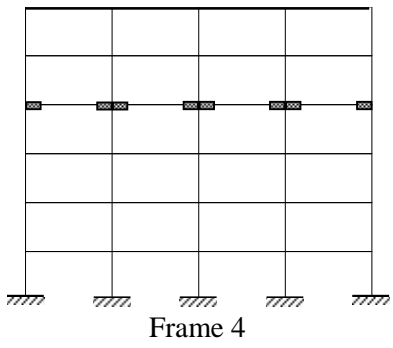
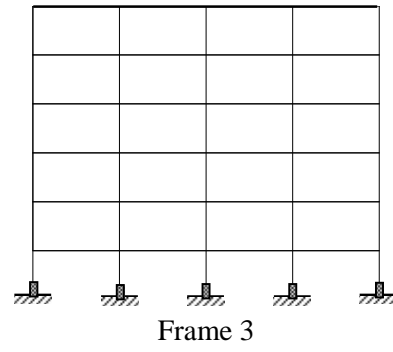
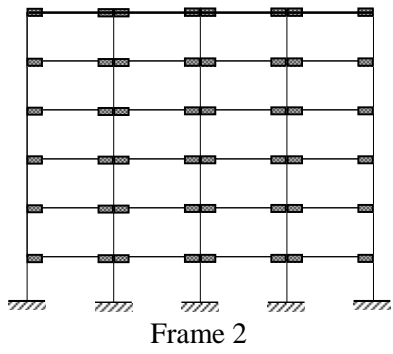


Loma Prieta (4.28 g)

Yielding ●  
Crushing x

Figure 7: Damage Scheme of Steel RC frame at collapse






SMA sections    

Figure 8: Locations of SMA bars

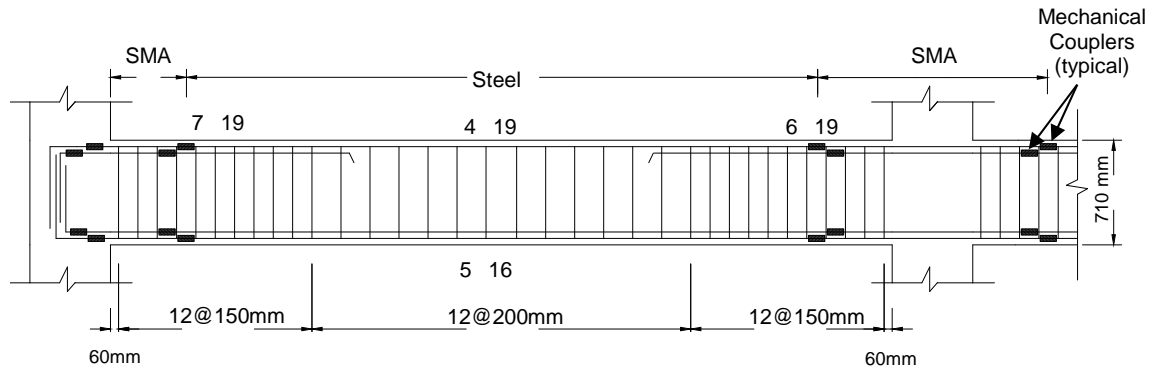


Figure 9: Reinforcement details of a typical SMA RC beam.

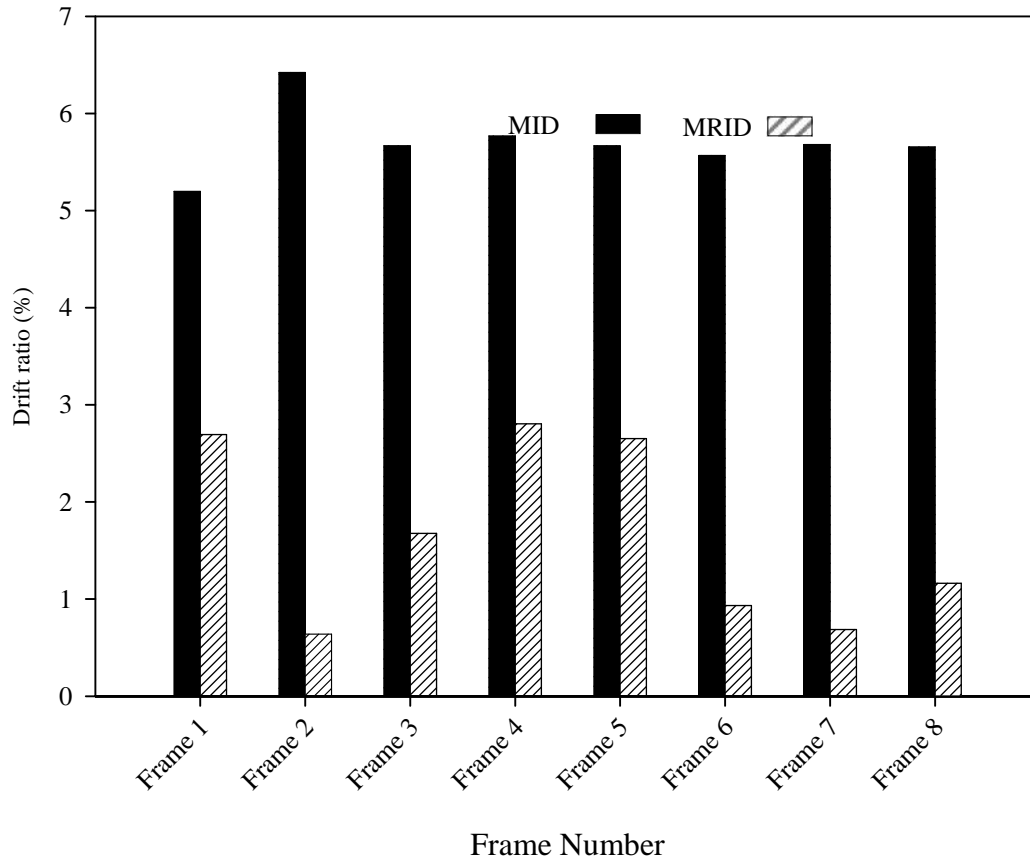
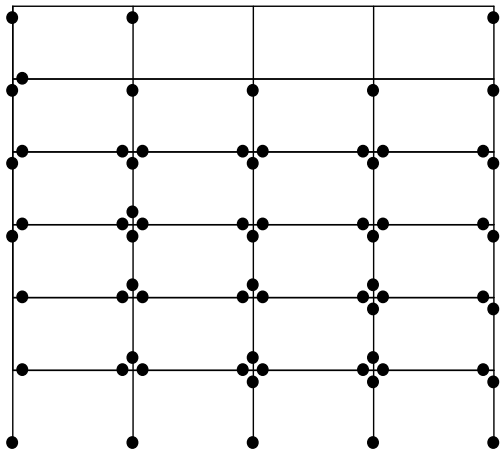
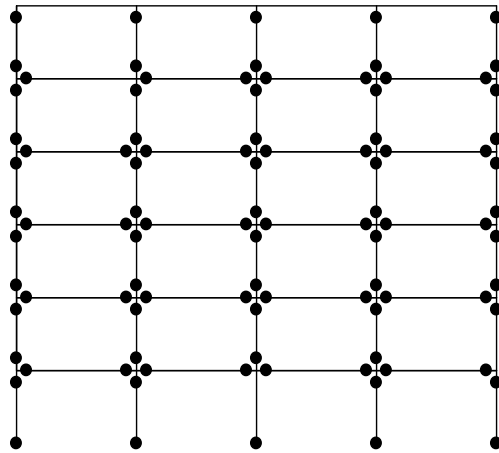


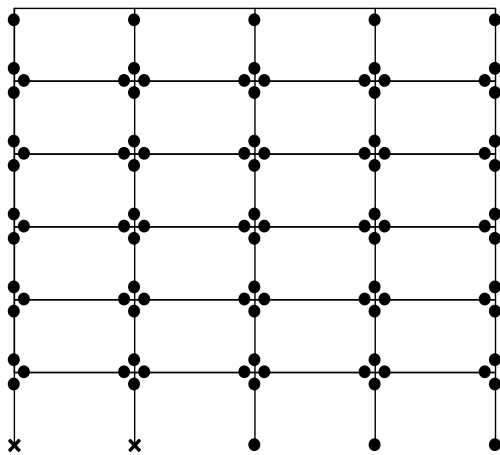
Figure 10: Average values of MID and MRID at  $S_a$  causing failure to the steel frame



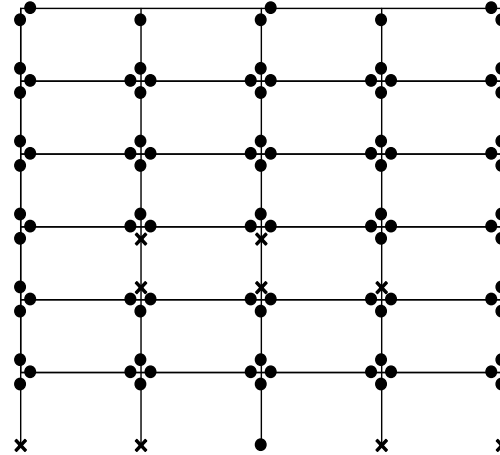
Imperial Valley 1.15g



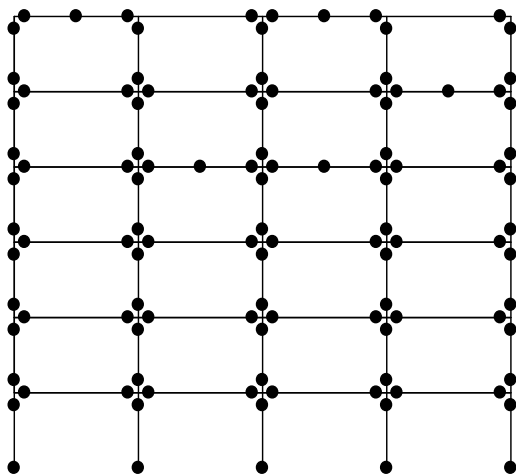
Northridge 2.6 g



San Fernando (8.15 g)



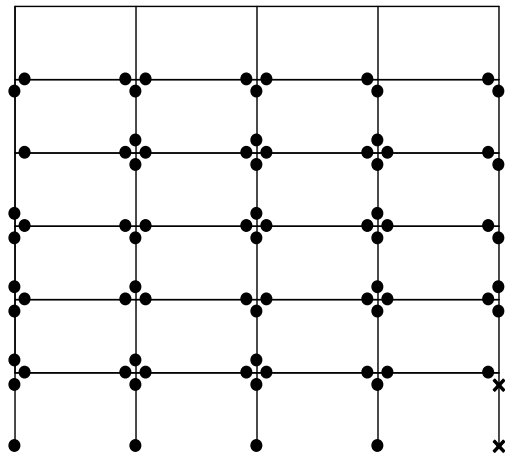
Whittier 5.00 g



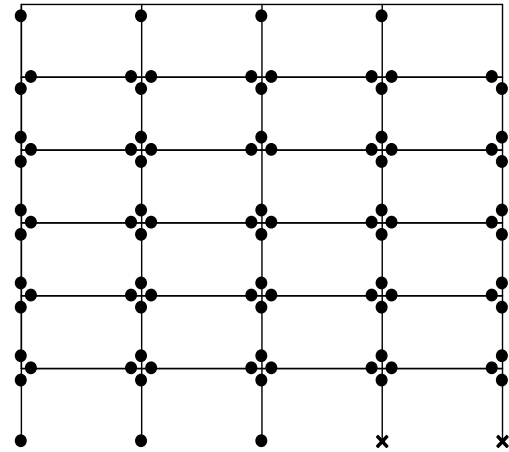
Loma Prieta 4.28g

Yielding     ●  
 Crushing    x

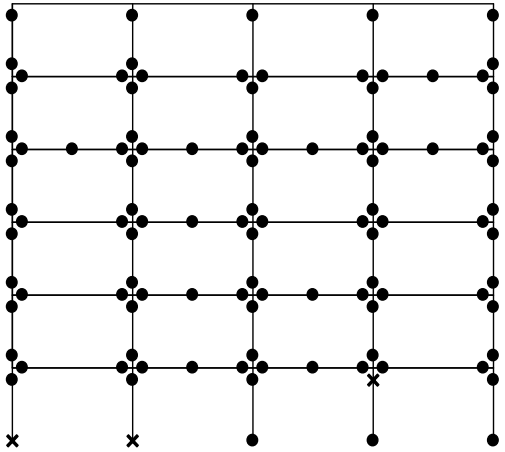
Figure 11a: Damage to Frame 2 (SMA at the ends of all beams)



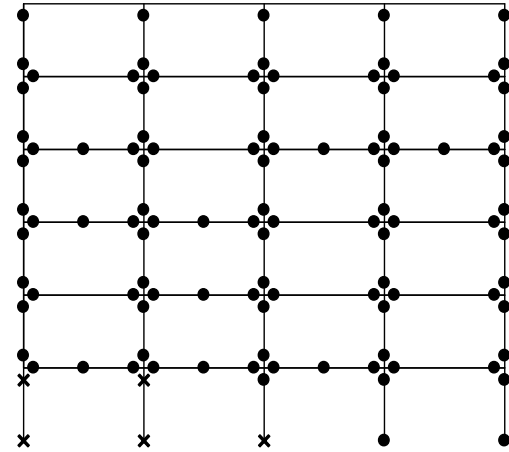
Imperial Valley 1.15g



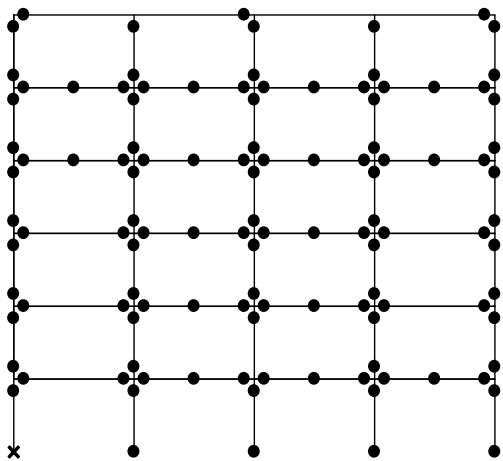
Northridge 2.6 g



San Fernando (8.15 g)



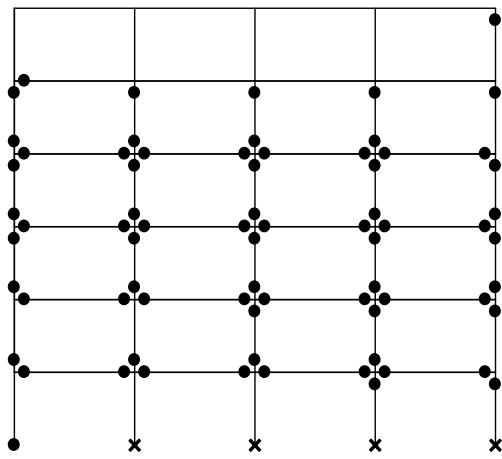
Whittier 5.00 g



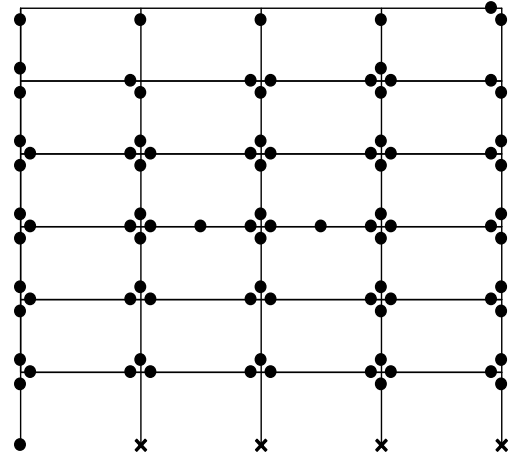
Loma Prieta 4.28g

Yielding     ●  
 Crushing    x

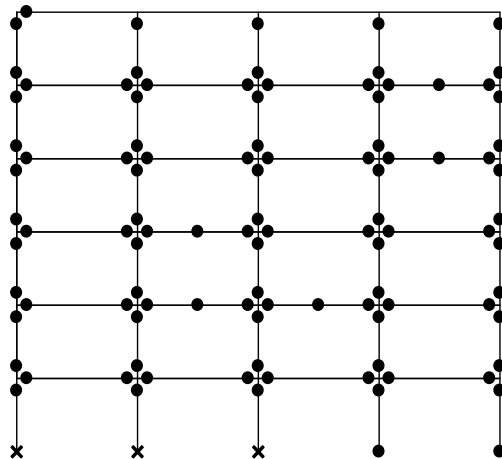
Figure 11b: Damage to Frame 3 (SMA at the lower ends of all the first storey columns)



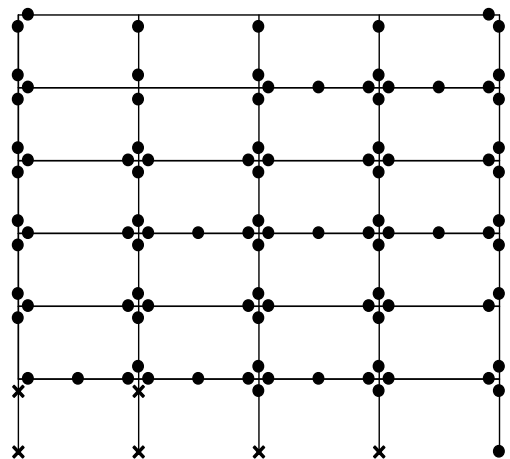
Imperial Valley 1.15g



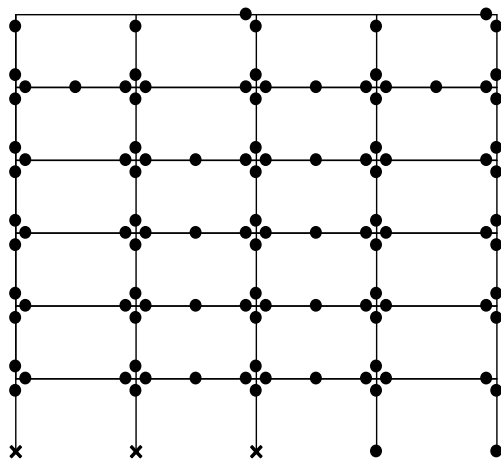
Northridge 2.6 g



San Fernando (8.15 g)



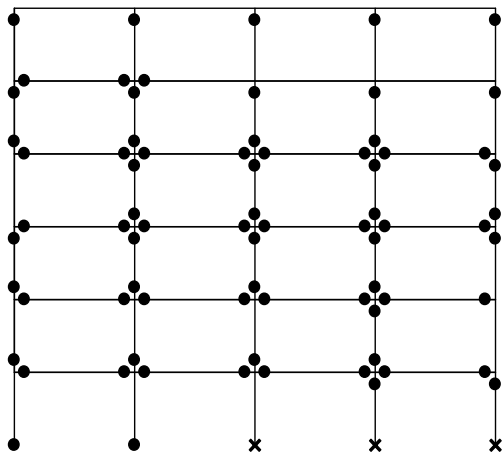
Whittier 5.00 g



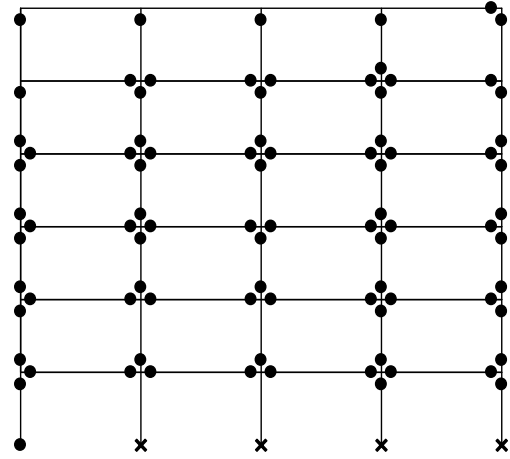
Loma Prieta 4.28g

Yielding     ●  
 Crushing    x

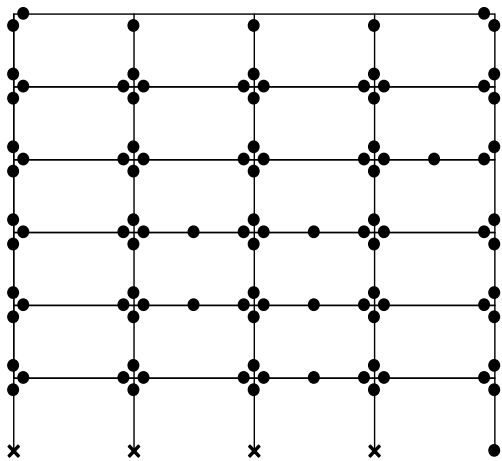
Figure 11c: Damage to Frame 4 (SMA at the ends of the fourth floor beams)



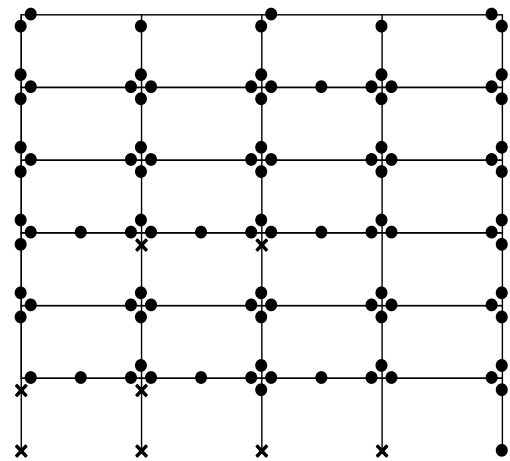
Imperial Valley 1.15g



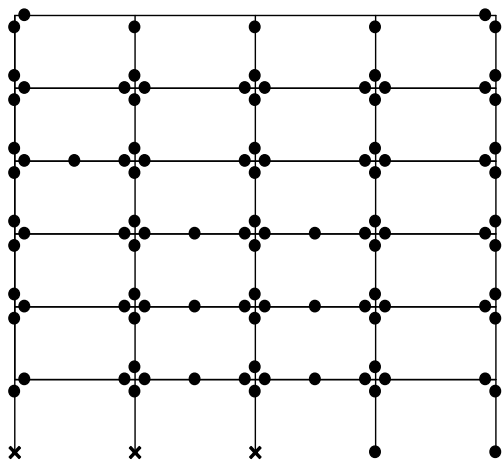
Northridge 2.6 g



San Fernando (8.15 g)



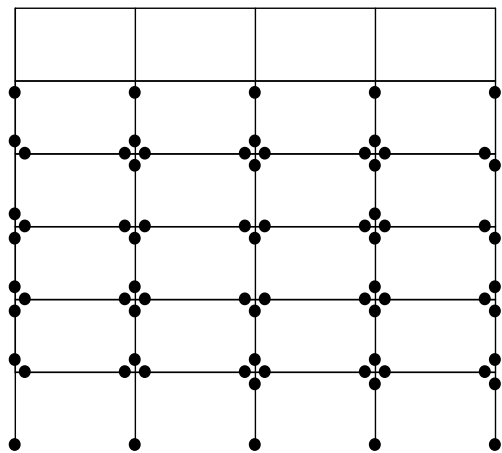
Whittier 5.00 g



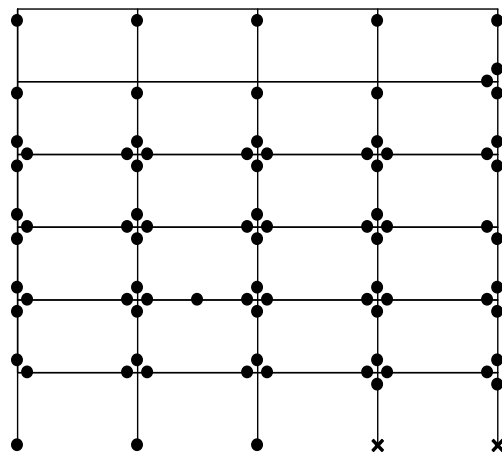
Loma Prieta 4.28g

Yielding     ●  
 Crushing    x

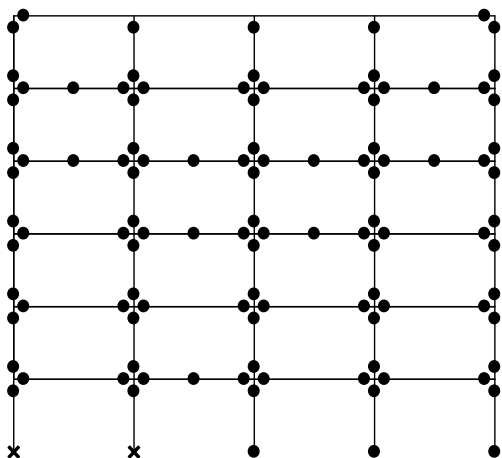
Figure 11d: Damage to Frame 5 (SMA at the ends of the fifth floor beams)



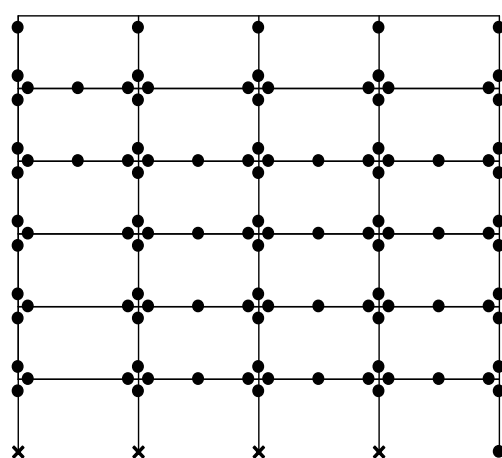
Imperial Valley 1.15g



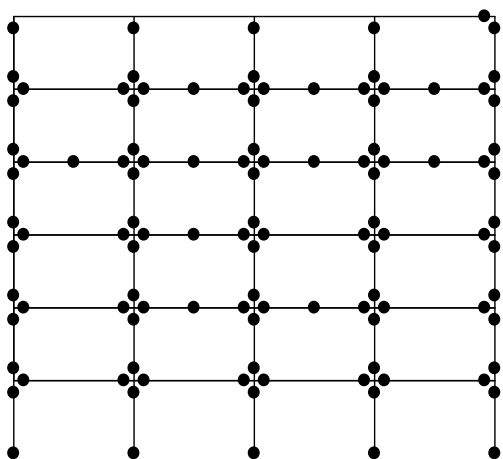
Northridge 2.6 g



San Fernando (8.15 g)



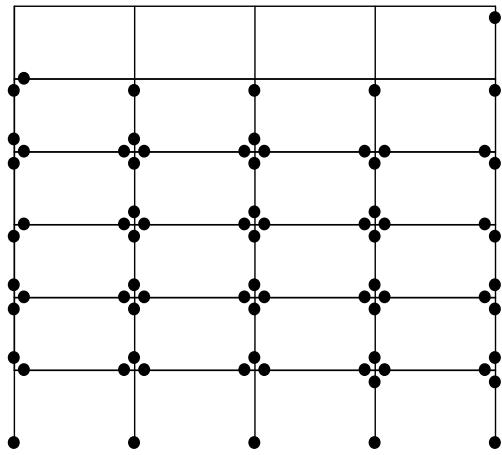
Whittier 5.00 g



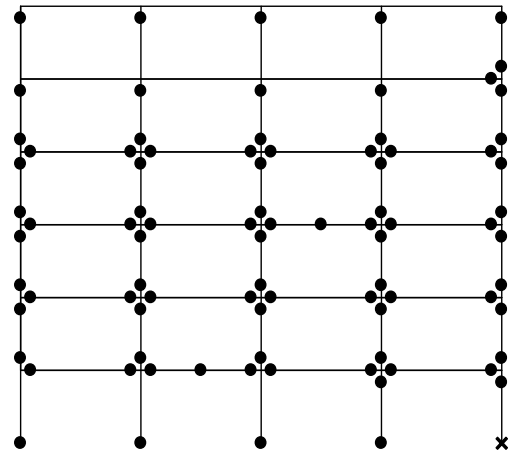
Loma Prieta 4.28g

Yielding     ●  
 Crushing     x

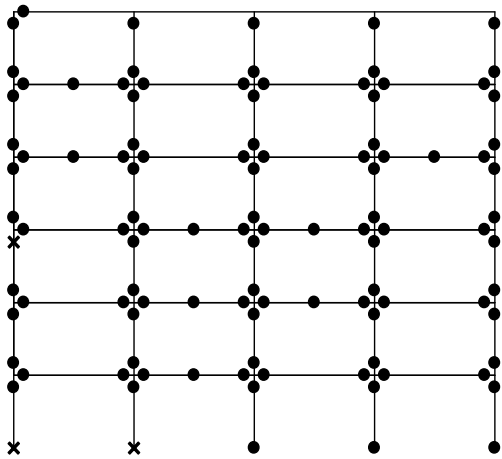
Figure 11e: Damage to Frame 6 (SMA at the ends of the first floor beams)



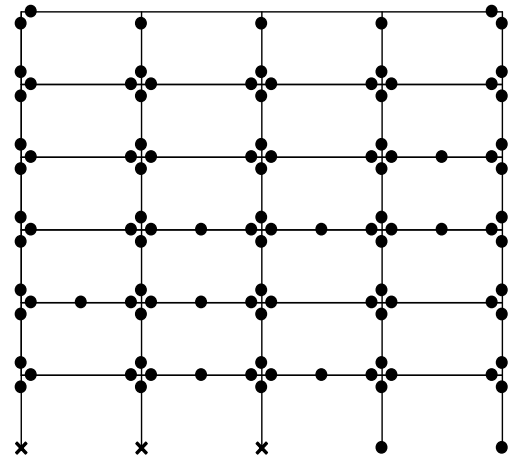
Imperial Valley 1.15g



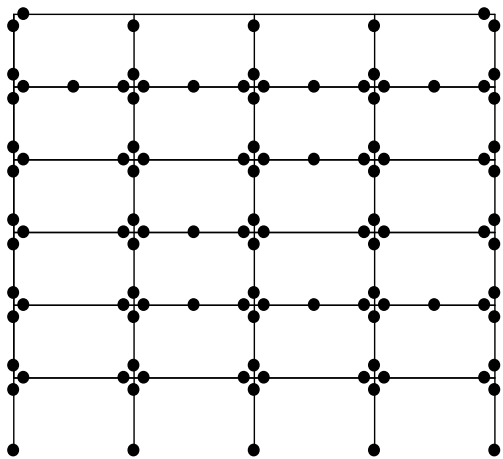
Northridge 2.6 g



San Fernando (8.15 g)



Whittier 5.00 g



Loma Prieta 4.28g

Yielding     ●  
 Crushing    x

Figure 11f: Damage to Frame 7 (SMA at the ends of the first and the fourth floor beams)



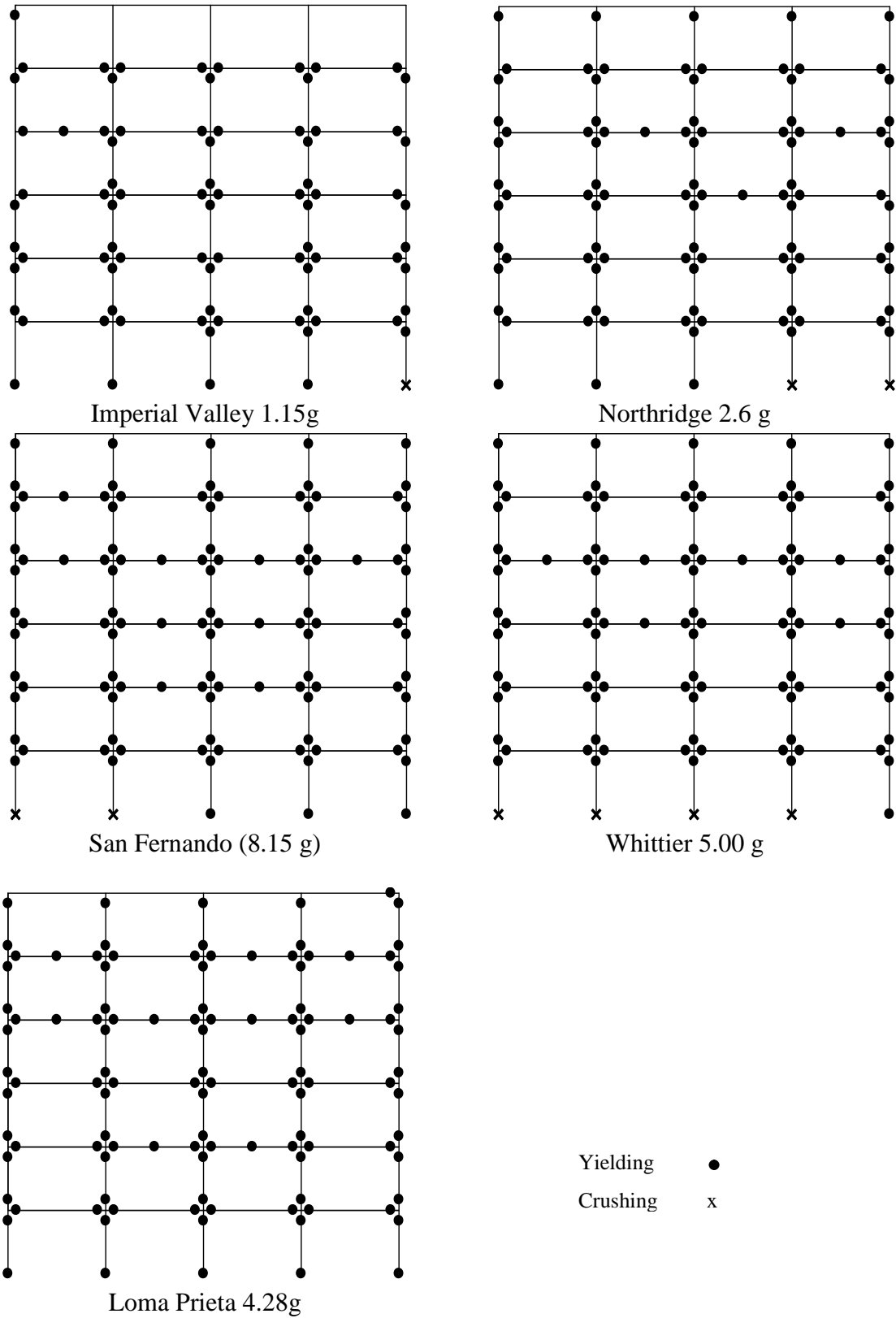
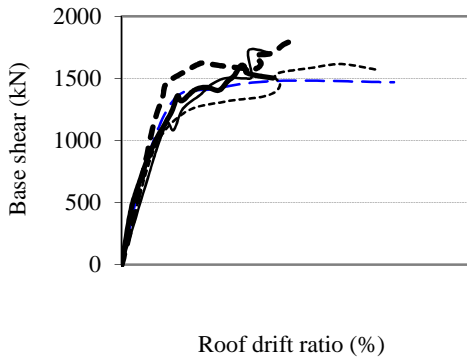
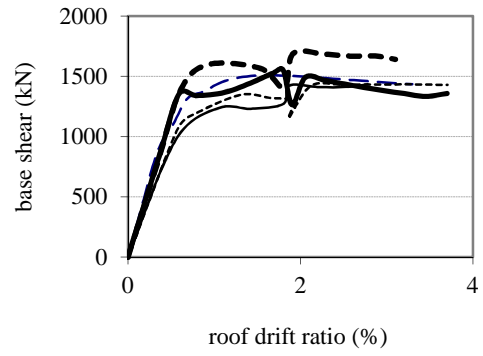


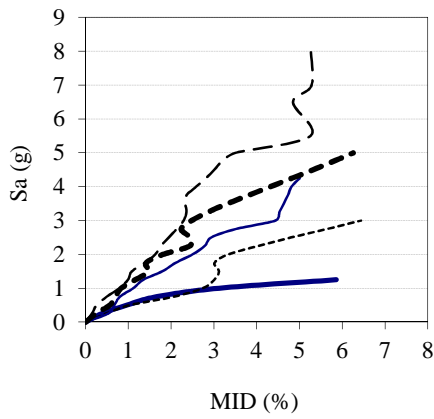
Figure 11g: Damage to Frame 8 (SMA at the first floor beams and columns)



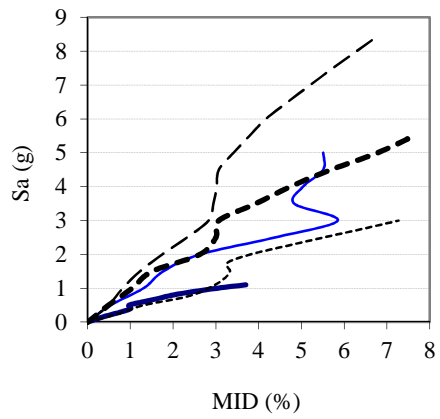
(a) Steel RC Frame (Frame 1)



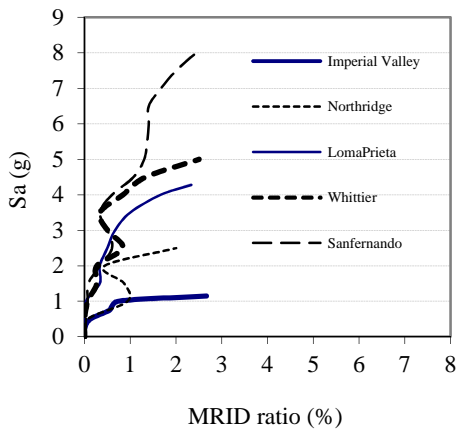
(b) SMA Frame (Frame 7)



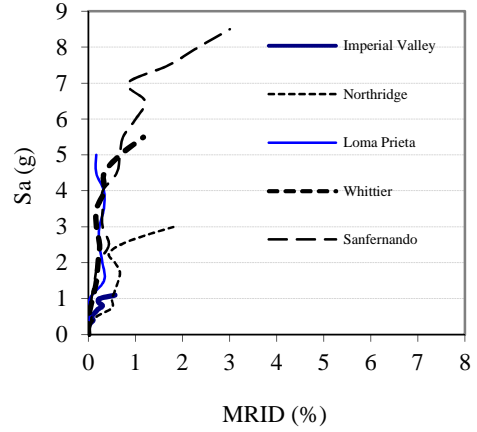
(c) Steel RC Frame (Frame 1)



(d) SMA Frame (Frame 7)

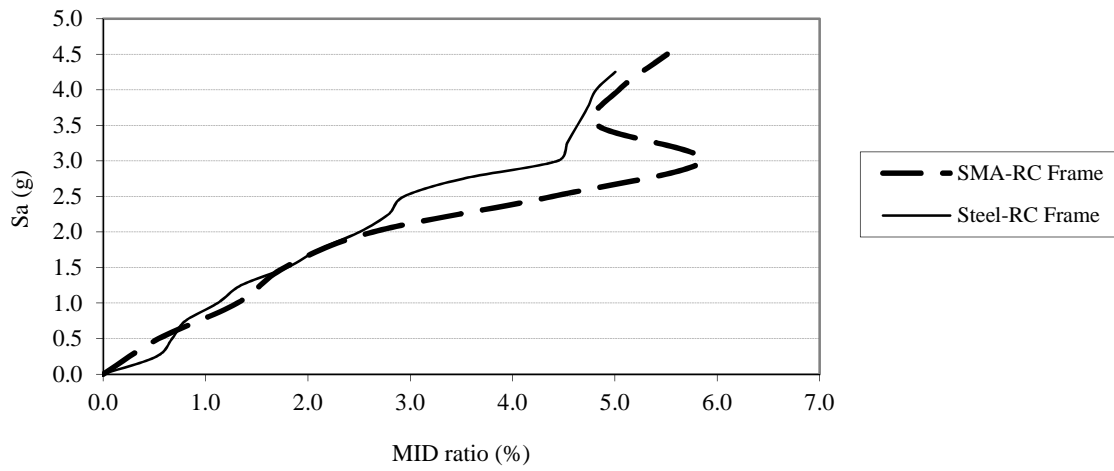


(e) Steel RC Frame (Frame 1)

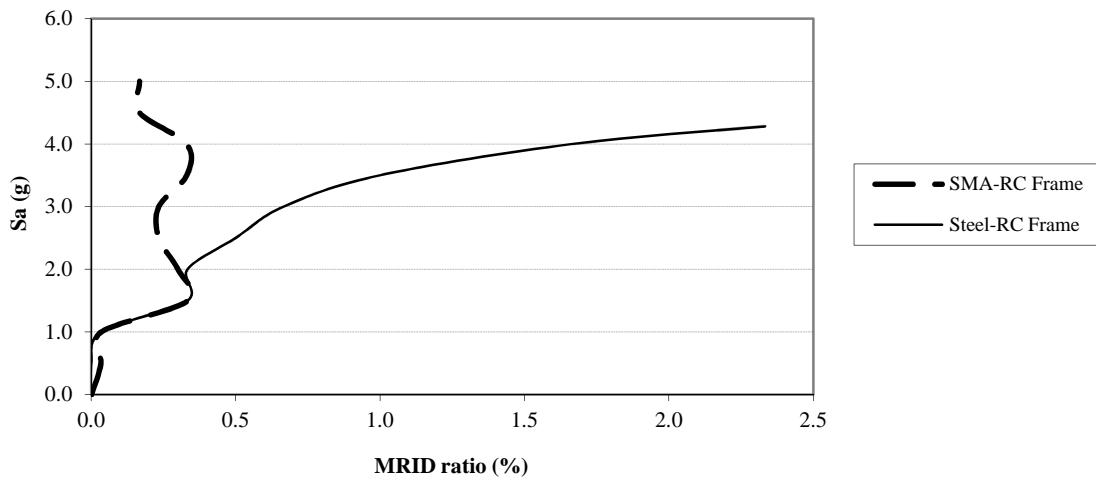


(f) SMA Frame (Frame 7)

Figure 12: IDA results

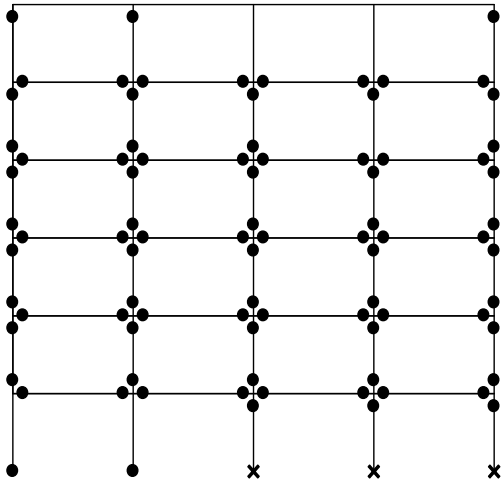


a) Variation of MID values during dynamic analysis (Loma Prieta record)

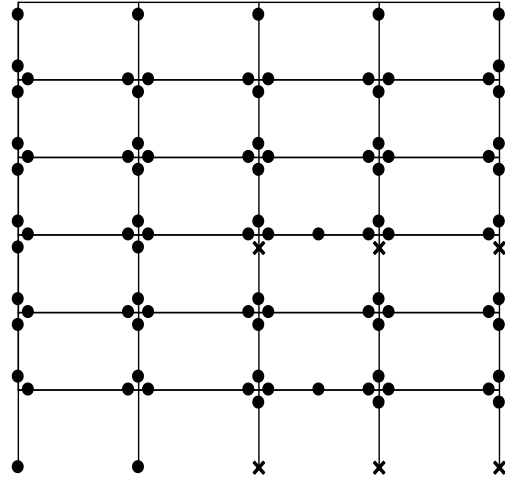


b) Variation of MRID values during dynamic analysis (Loma Prieta record)

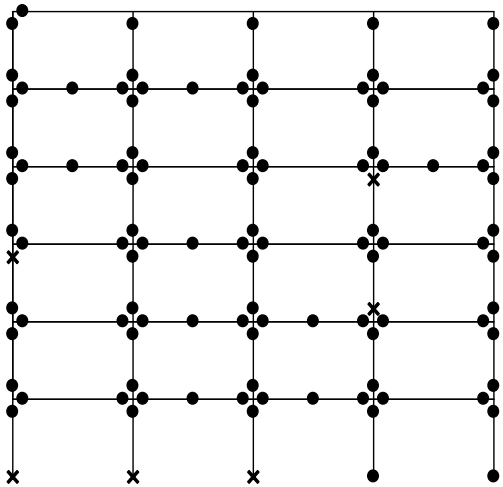
Figure 13: Variation of drift values during the IDA considering Loma Prieta record



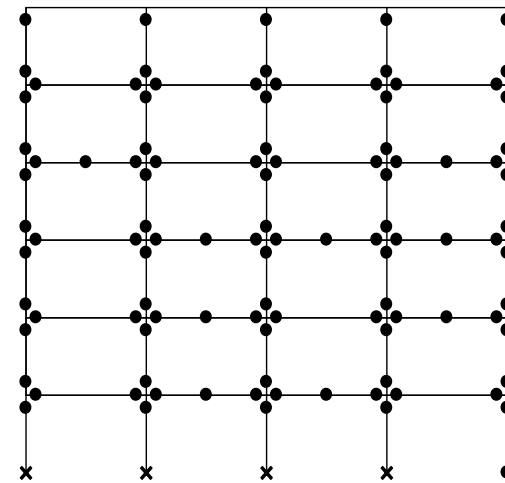
Imperial Valley 1.28g



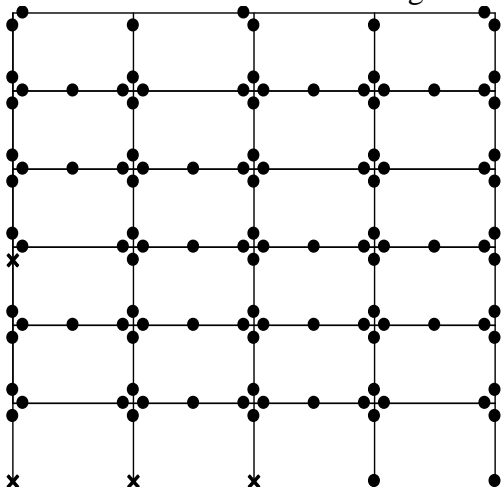
Northridge 3.10 g



San Fernando 8.90g



Whittier 5.25 g



Loma Prieta 5.75g

Yielding     •  
 Crushing    x

Figure 14: Damage scheme of Frame 7 at collapse